INT. J. NUM. METH. HEAT FLUID FLOW, VOL. 2, 3–20 (1992)

FINITE ELEMENT—ALGEBRAIC CLOSURE MODELLING OF TURBULENT SEPARATED FLOW OVER A BACKWARD-FACING STEP: STEADY AND UNSTEADY ASPECTS

ZHONG QIN AND M. D. OLSON

Department of Civil Engineering, University of British Columbia, Vancouver, B.C., V6T 1W5, Canada

ABSTRACT

A numerical method is developed for steady and unsteady turbulent flows with significant regions of separation. A finite element formulation of the Navier–Stokes equations with a modified Baldwin–Lomax eddy viscosity closure is used. The method of averaging is employed to obtain a periodic solution of unsteady flow. The formulation is tested on a problem of flow over a backward-facing step and the results are compared with experimental and other numerical results. The gross features of both steady and unsteady flows are reasonably well predicted by the numerical analysis, at least for the limited range of parameters tested so far.

KEY WORDS Turbulent flow separation Closure modelling Baldwin–Lomax eddy viscosity

INTRODUCTION

Turbulent flow separation has received a great deal of attention because of its practical importance. It may be present in many practical machines and devices, thus reducing their performance; nevertheless, it is still far from well understood. Simpson[1] has presented a detailed discussion of experimental and computational work on two-dimensional turbulent separated flows, which was followed more recently by an updated review[2]. There appears to be no generally accepted method to calculate such flows, especially for the unsteady case.

Although the flow over a backward-facing step is one of the simplest separated-reattaching flows, the flow field is still very complex. It includes all the significant features of the general problem and hence it is one of the standard test cases of complex turbulent flows[3]. As a consequence, numerous studies of this basic flow have been conducted for the steady case. Experimental investigations have been performed by a number of researchers for different flow conditions[4,5] and the k–ε turbulence model has been widely used for numerical prediction[6–8].

Relatively little effort, however, has been devoted to unsteady turbulent flow over a backward-facing step. Two experimental studies show that this type of separated flow has very complex flow characteristics. Brocher[9] reported that Lebouché and Martin pulsed the mean velocity of the flow in a duct which had enlargements on both sides and thus produced symmetrical separated regions. The amplitude $\tilde{U}_0$ of the pulsation was up to 30% of the mean velocity $\bar{U}_0$ and the frequency F ranged from 3 to 23 Hz. The gross flow characteristics were dependent on a reduced frequency parameter $F^* = Fh/\bar{U}_0$, where h is the step height. It was reported that for high pulsation rates, there existed a critical frequency $F_c^* \approx 0.07$ such that (a) if $F^* < F_c^*$, the recirculation vortex was shed, (b) if $F^* \approx F_c^*$, the vortex was very unstable and

0961–5539/92/010003–18$2.00

Received March 1991
Revised June 1991

(c) if $F^* > F_c^*$, the vortex was stable but was smaller than for steady flow. Mullin *et al.*[10] made a systematic experimental study of a pulsating flow over a step where $F^* = 0.007$ and $\tilde{U}_0/\bar{U}_0 = 0.12$ for a 1 Hz sinusoidal velocity oscillation. It was observed that the stability of the separated flow region behind the step was strongly perturbed by the free-stream oscillations and that the position of reattachment was dependent on the phase of the free-stream velocity. Shedding of the recirculation vortex was reported to take place. Unfortunately, no Reynolds shear stress or other flow structure measurements were made to lead to a conclusive explanation of the shedding process.

In the present work, an attempt is made to develop a capability to model unsteady turbulent separated flows with the simplest possible representation. A finite element representation of the Navier–Stokes equations with an algebraic closure model for eddy viscosity is adopted. The Baldwin–Lomax eddy viscosity model is appropriately modified for these challenging cases. The method of averaging is applied to obtain a periodic solution and thereby avoid costly numerical integration in time. The method is applied to the example of flow over a backward-facing step. Numerical predictions for the steady case are in good agreement with experimental data, and preliminary results for unsteady flow reproduce the main features of the experimental observations and show that the present method has considerable potential. As far as the authors are aware, this is the first reported investigation of applying these techniques to unsteady separated turbulent flow.

THEORETICAL FORMULATION

The Reynolds averaged momentum and continuity equations for two-dimensional incompressible turbulent flow are given by:

$$\begin{aligned} \rho(u_{,t}+uu_{,x}+vu_{,y}) &= -p_{,x}+2(\mu_e u_{,x})_{,x}+[\mu_e(v_{,x}+u_{,y})]_{,y} \\ \rho(v_{,t}+uv_{,x}+vv_{,y}) &= -p_{,y}+2(\mu_e V_{,y})_{,y}+[\mu_e(V_{,x}+U_{,y})]_{,x} \\ u_{,x}+v_{,y} &= 0 \end{aligned} \tag{1}$$

where x, y are the coordinates and u, v are the ensemble-averaged velocity components in x, y, respectively, t is the time, ρ is the fluid density, p is the pressure, μ_e is the effective viscosity made up of the molecular viscosity μ and the eddy viscosity μ_t.

The linear unsteady velocity terms in (1) must be included in unsteady flow calculations. Since usually calculations must proceed in time as well as in two spatial dimensions, care is needed to avoid numerical instability and to minimize computation time, especially when flow reversal occurs.

The present work uses curved isoparametric finite elements with bi-quadratic interpolation for velocities and bi-linear for pressure. The velocities and pressure are represented by:

$$\begin{aligned} u &= \sum_{j=1}^{8} N_j u_j(t) \\ v &= \sum_{j=1}^{8} N_j v_j(t) \\ p &= \sum_{j=1}^{4} M_j p_j(t) \end{aligned} \tag{2}$$

where N_j M_j are the shape functions, and u_j, v_j and p_j are the time-dependent nodal variables.

Upwinding is essential to obtain converged solutions for the high Reynolds numbers encountered in this study. The streamline upwind technique previously developed for linear elements[11] and extended to quadratic elements[12] is used to stabilize the calculations at high Reynolds numbers. Instead of the common Galerkin method in which weighting and interpolation

functions are from the same class of functions, the streamline upwind/Petrov–Galerkin formulations are constructed by using the upwind weighting function:

$$W_i = N_i + \tilde{\kappa}(uN_{i,x} + vN_{i,y})/\|u\|^2 \qquad i = 1, 2, \ldots, 8 \tag{3}$$

where $\tilde{\kappa}$ is the upwind parameter[12] and $\|u\|^2 = u^2 + v^2$. In the present work, only partial upwinding[12] is employed. That is, the upwind modification in the weighting function (3) is only applied to the convective and transient terms. By substituting the interpolation functions (2) into (1), employing the method of weighted residuals with the weighting function (3), and integrating the diffusive terms by parts once, the upwind finite element equations are obtained as:

$$\mathbf{M}\dot{\mathbf{d}} + \mathbf{K}\mathbf{d} + \delta = \mathbf{0} \tag{4}$$

where $\mathbf{M}$ is the mass matrix, $\mathbf{K}$ is the stiffness matrix, δ contains the non-linear terms due to the convection terms in (1), and $\mathbf{d}$ is the nodal vector of unknowns. Details of all matrices are given in the Appendix.

The direct time integration solution of the resulting finite element equation (4) is time consuming and expensive. Because periodic flow is by far the most common time-dependent motion, in the present study, the need for the numerical integration in time is eliminated by assuming the solution to be periodic and applying the method of averaging. We assume that the nodal vector of unknowns $\mathbf{d}$ takes the periodic form.

$$\mathbf{d} + \mathbf{A} + \mathbf{B}\cos(\Omega t) + \mathbf{C}\sin(\Omega t) \tag{5}$$

where $\mathbf{A}$, $\mathbf{B}$ and $\mathbf{C}$ are constant vectors, and Ω is the oscillating frequency. In (5), the nodal vector is composed of a mean component $\mathbf{A}$ and a periodic component with in-phase and out-of-phase amplitudes $\mathbf{B}$ and $\mathbf{C}$, respectively. Thus,

$$\dot{\mathbf{d}} = -\mathbf{B}\Omega\sin(\Omega t) + \mathbf{C}\Omega\cos(\Omega t) \tag{6}$$

To obtain the three sets of equations for the three sets of unknowns $\mathbf{A}$, $\mathbf{B}$ and $\mathbf{C}$, (5) and (6) are first substituted into the finite element equation (4), then the resulting equations are: (1) averaged over the period $2\pi/\Omega$; (2) multiplied by $\cos(\Omega t)$ and averaged over the period $2\pi/\Omega$; (3) multiplied by $\sin(\Omega t)$ and averaged over the period $2\pi/\Omega$. Through this process, a set of non-linear algebraic equations for $\mathbf{A}$, $\mathbf{B}$ and $\mathbf{C}$ is obtained:

$$\begin{bmatrix} \mathbf{K} & 0 & 0 \\ 0 & \mathbf{K} & \Omega\mathbf{M} \\ 0 & -\Omega\mathbf{M} & \mathbf{K} \end{bmatrix} \begin{Bmatrix} \mathbf{A} \\ \mathbf{B} \\ \mathbf{C} \end{Bmatrix} + \begin{Bmatrix} \delta_{\mathbf{A}} \\ \delta_{\mathbf{B}} \\ \delta_{\mathbf{C}} \end{Bmatrix} = 0 \tag{7}$$

where $\delta_{\mathbf{A}}$, $\delta_{\mathbf{B}}$ and $\delta_{\mathbf{C}}$ are given in the Appendix. These equations are solved using the Newton–Raphson procedure.

The use of (5) implies that the periodic motion can be approximated by a steady term and the first harmonic. This should be a good approximation for those cases where the oscillating component is small with respect to the steady one. This idea is supported by experimental evidence[18], where it was observed that the time variation of the downstream flow was similar to that at the inlet.

TURBULENCE MODEL

One of the main difficulties in solving the turbulent Navier–Stokes equations (1) is to describe the eddy viscosity μ_t reasonably. It is now possible to apply a variety of complex turbulence models to simulate turbulent flows as a result of increases in computer capability. Algebraic eddy viscosity models, however, are still very popular for engineering calculations, since their implementation results in minimum requirements of computer time and storage. The Baldwin–Lomax algebraic eddy viscosity model has found wide application in the prediction of

steady turbulent flows[13–15]. The present authors have tested this model and found that it is well behaved for attached flows[16] and with appropriate modifications, it can represent separated flows as well[12].

Steady flow calculation models and methods have been extended to unsteady turbulent flow[17–19]. A number of investigators have argued that, as long as the period of the organized unsteadiness is relatively long compared with the turbulence timescales, it should be acceptable to use the approximation that the turbulent structure is unaffected by the unsteadiness[2]. Some experimental investigations have shown that unsteadiness does not alter the turbulence structure much from that for steady flows, except perhaps in large amplitude oscillation cases[1]. For moderate amplitude oscillations (velocity amplitude/mean velocity <0.37), Cousteix *et al.*[18] have shown that the turbulent shear stress is independent of phase angle and has values corresponding to steady turbulent flows. All moderate amplitude measurements indicate that outside of the near-wall region the turbulence structure is basically unaffected by organized unsteadiness.

Many numerical predictions of unsteady turbulent flows have indicated that the turbulent closures developed for steady flows are still valid for unsteady flows[17–19]. Cebeci[20] concurred that the ability of a turbulence model to simulate unsteady flows can be gauged by its ability to simulate steady flows. Unsteadiness relieves none of the numerical and turbulence model difficulties encountered with steady free-stream separation. As mentioned above, the Baldwin–Lomax eddy viscosity model works well for steady flow, especially, the modified version which has the capability to simulate separated flows. A recent calculation of turbulent oscillating channel flows yielded satisfactory results by using the Baldwin–Lomax model[21]. The present test case, turbulent flow over a backward-facing step, is a challenging one for the Baldwin–Lomax model. Because a large separation zone exists, it is difficult to determine the length scale in the original outer formulation and to simulate the backflow region[12,15]. The modifications made previously[12] appear to be very important. A brief summary of the modified Baldwin–Lomax model follows. Further details are available in Reference 12.

The modified Baldwin–Lomax model provides an algebraic representation of the eddy viscosity as a function of y, the coordinate normal to a wall. It is subdivided into three functions, namely an inner one close to the wall, an outer one in the outer flow and an algebraic model for back flow in order to approximate the distinctly different mixing phenomenon taking place in the respective regions. In the inner region, the eddy viscosity is given by:

$$(\mu_t)_{\text{inner}} = \rho(kyD)^2|\omega| \tag{8}$$

where ρ is the density, $|\omega|$ is the magnitude of the vorticity, $k=0.4$, the von Karman constant, y is the normal distance from the wall, D is the Van Driest damping factor, which is given by:

$$D = 1-\exp(-y\sqrt{\rho\tau_w^*}/26\mu) \tag{9}$$

where τ_w^* is the larger of the magnitude of the wall shear stress and the maximum shear stress at a given streamwise location, and μ is the molecular viscosity. In the outer region, the eddy viscosity is given by:

$$(\mu_t)_{\text{outer}} = \rho K C_{cp} F_{\text{wake}} F_{\text{kleb}} \tag{10}$$

where $K=0.0168$ is the Clauser constant, C_{cp} is an additional constant which is taken as 1.2, and

$$F_{\text{wake}} = Y^*_{\max} F_{\max} \tag{11}$$

The quantities $Y^*_{\max}$ and $F_{\max}$ are determined from the outer function:

$$F(y^*) = y^*|\omega|D \tag{12}$$

where $y^* = y$ for attached flow, and $y^* = y - y_b$ for separated flow, where y_b is the distance from the backflow edge (where the tangential velocity $u_t = 0$) to the wall. $F_{\max}$ is the maximum value of $F(y^*)$ that occurs in a profile and $Y^*_{\max}$ is the value of y^* at which $F_{\max}$ occurs. In (10), the

function F_{kleb} is the Klebanoff intermittency factor given by:

$$F_{kleb}=[1+5.5(C_{kleb}y^*/y^*_{max})^6]^{-1} \tag{13}$$

where C_{kleb} is an empirical constant which is taken as 0.54. In the backflow region, the eddy viscosity is calculated by using the Goldberg backflow model[22] which is too involved to reproduce here. The theory of the model and its application to separated turbulent flows have been given elsewhere[15,22]. The turbulent eddy viscosity is switched, for an attached profile, from the inner to the outer formulation at the location where the values from (8) and (10) are equal; for a separated profile, from the backflow to the outer formulation at the location where $y=y_b$.

METHOD OF SOLUTION

The finite element method and the modified turbulence model are combined in a new program. The resulting non-linear equations are solved using the Newton–Raphson method. The effective viscosity μ_e is kept constant when the Newton–Raphson iterations are performed since its dependence on the velocity is too complicated to include. Hence μ_e is only updated at specified times in the calculations. The relaxation technique[12] is employed to calculate the eddy viscosity and to speed up the solution convergence. A uniform eddy viscosity field is first established from an appropriate laminar solution. Then several Newton–Raphson iterations are performed on the velocity–pressure variables with eddy viscosity held constant. Once the velocity–pressure field has converged, the turbulence model is invoked and the viscosity distribution is updated by the relaxation formulation[12]. Then the velocity–pressure calculations are repeated with the new eddy viscosity distribution. The process is continued until the viscosity has converged as well. This process is controlled by specified accuracy tolerance levels which are progressively reduced as the solution approaches the final required results. The procedure of calculation has been shown to be very efficient compared to the usual method of proceeding from low to high Reynolds numbers step by step.

In the present work, all matrices are evaluated by 3×3 Gauss numerical integration, and all the calculations for the turbulent viscosity are carried out at the Gauss points. Because the eddy viscosity is affected only by velocity gradients and not by velocity oscillations, for simplification, the vorticity and the wall shear stress in the Baldwin–Lomax formula are calculated only from the distribution of the mean component of velocity (i.e. part A in (5)). Similarly, the upwind modification terms in the weighting function (3) are calculated based on the mean component of velocity as well. The computer program is implemented in double precision on a new super computer system with vector facility, namely an IBM model 3090. The solution of the linear algebraic equations and the matrix inversions are performed using a sparse matrix solving package called SPARSPAK.

Once the above solution process has finished, subsequent calculations are performed to obtain instantaneous streamline plots and reattachment lengths X_r. That is, for particular values of the phase angle ϕ over one cycle of basic motion, the instantaneous velocity field is calculated from (5). A finite element program[23] is used to solve for the stream function from the known vorticity distribution. At the same time, the reattachment point is determined by calculating the shear stress on the wall and finding the first point downstream of the step where it vanishes. The minimum and maximum values of X_r as a function of ϕ are then easily determined.

NUMERICAL RESULTS AND DISCUSSION

Steady flow

The flow problem under consideration and the finite element grid used are shown in *Figures 1* and *2*, respectively. The aspect ratio of the backward-facing step height h to the overall cross-sectional width is 1:3. For the present calculations, the following boundary conditions

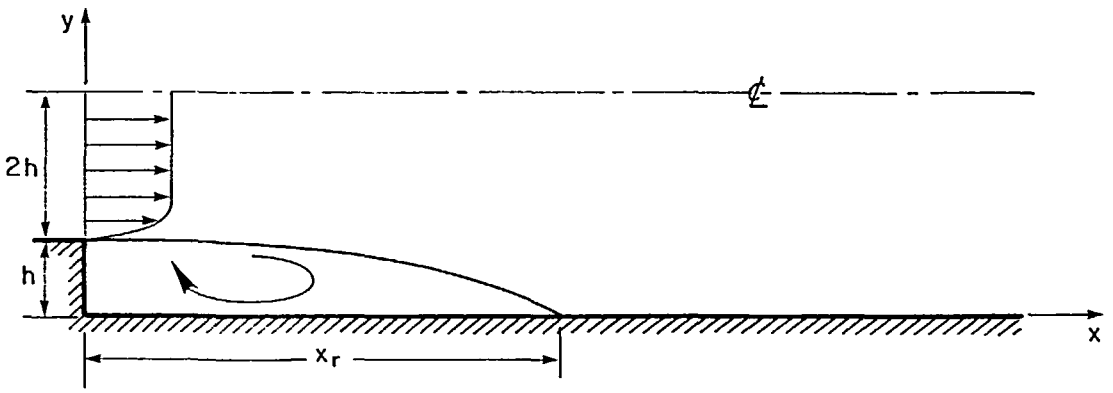

Figure 1 Flow configuration

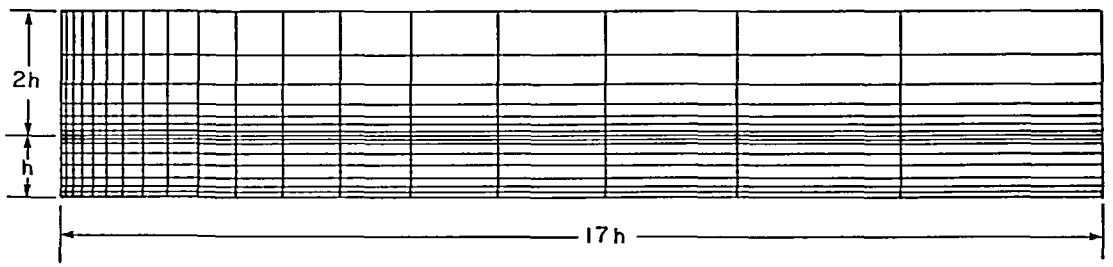

Figure 2 Finite element grid for steady flow

have been adopted:

	$u=0, y \leqslant h,$	
Upstream:	$u=u_0, y>h,$	$v=0$
Downstream:	$p=0,$	$v=0$
At the wall:	$u=0,$	$v=0$
At the symmetry line:	$\tau=0,$	$v=0$

where u_0 is the free-stream velocity. At the upstream boundary, the u velocity increases from zero to u_0 linearly over one element. Other versions of this boundary condition were also tried such as using a fully developed turbulent profile but it was found that the overall solution and, in particular, the reattachment length were hardly affected by such changes. Hence, the simpler boundary condition was used for most of the results reported here.

Considering the boundary condition on the top boundary, solutions have been presented in the literature for two different versions, namely, a zero-slip wall and a frictionless symmetry line. In the present work, we have chosen the latter mainly for computational ease since this case has no boundary layer to be modelled there. This boundary condition does affect the recirculation flow and the reattachment length, but since the present work was mainly of an exploratory nature, this was not considered important.

The detailed dimensions for the finite element grid are given in *Table 1*. The various element dimensions were calculated by geometric progression as indicated. Grid dependency was checked by calculations on a coarser mesh, the results from which compared favourably with those from the finer grid. Further, the results obtained for the steady case with the present grid apparently

Table 1 Details of finite element grid (shown in *Figure 2*)

Number of elements		Element dimensions				
x	y	Δx_{min}	$\Delta x_i/\Delta x_{i-1}$	Δy_{min}	$\Delta y_i/\Delta y_{i-1}$*	$\Delta y_i/\Delta y_{i-1}$**
18	15	0.0945 h	1.232	0.063 h	1.482	1.495

* $y<h$ from $y=0^+$ 4 elements, from $y=h^-$ 4 elements.
** $y>h$ from $y=h^+$ 7 elements.

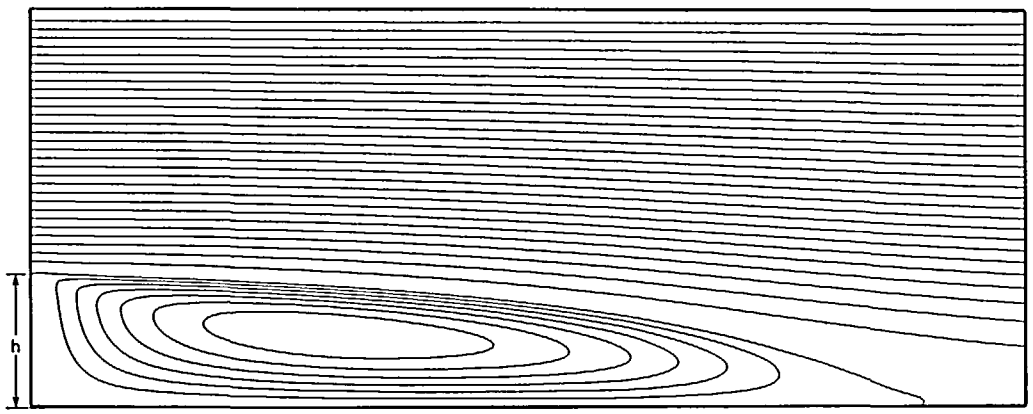

Figure 3 Streamline contours of steady flow with aspect ratio 1:3

compared reasonably well with other numerical predictions and, therefore, it was felt that the grid was adequate for the present purpose which was mainly to explore the potential of the proposed method for the unsteady problem.

Computations were performed for two Reynolds numbers, namely, 52000 and 69160, based on the free-stream velocity u_0 and the step height h. The latter represents the same flow condition as in Sohn[6] and Kim *et al.*[4]. As in the experimental case[4], the effect of change in Reynolds number over a limited range was found to be negligible. Hence, only the results for $Re=69160$ are presented here.

Figure 3 shows the streamline contours obtained from this calculation. The most important parameter for comparison with the experimental data of Kim *et al.*[4] is the reattachment length X_r of the separation zone behind the step. The accepted experimental measurement of X_r is 7.0 ± 1.0 h. The predicted value in the present study is about 6.7 h. Sohn[6] predicted X_r as 5.59 h using a k–ε model and the finite element method with the BTD-type streamline upwinding. The fact that the present result is larger than Sohn's is consistent with the different top boundary condition.

In *Figure 4*, the predicted velocity profiles are compared with the experimental measurements and the computed results of Sohn. The predictions agreed reasonably well with the experimental data except very near the wall. Both predictions show a slower recovery downstream of the reattachment point, but this is common to most other computations as well[6,7].

Figure 5 shows a comparison of the computed pressure coefficient C_p on the wall with the experimental data. The pressure distribution reproduces fairly well the trends of the experimental measurement and is comparable to the prediction of Reference 6. Hence, it seems fair to conclude that the results from the present model compare favourably with experimental and other numerical ones for the steady case.

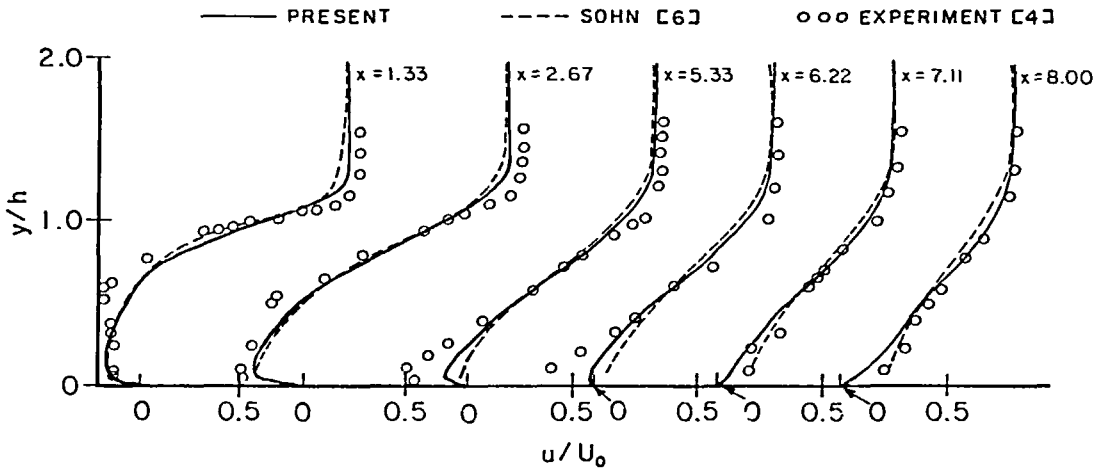

Figure 4 Velocity profiles of steady flow

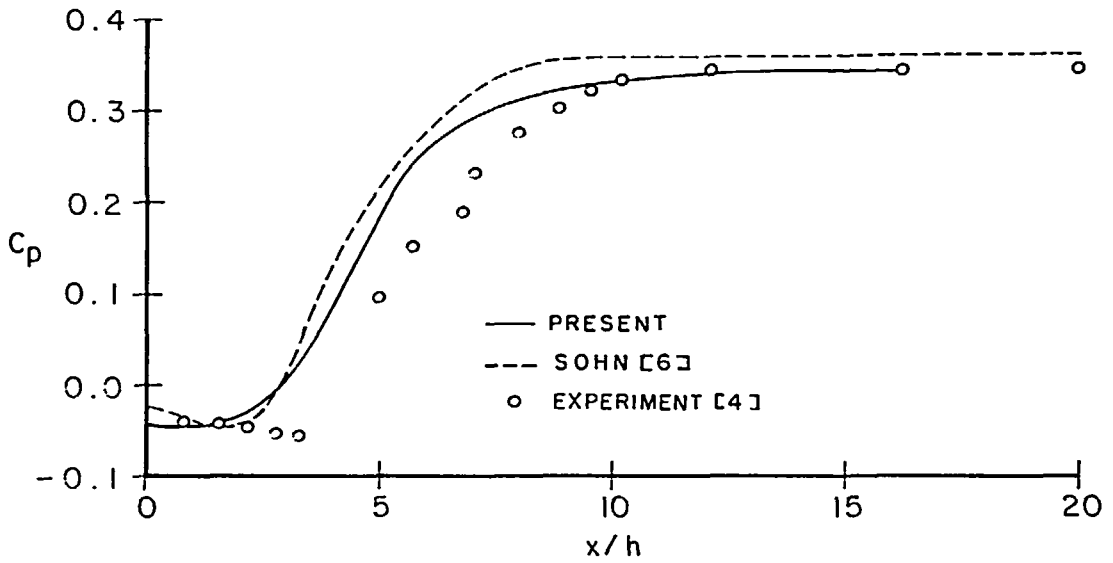

Figure 5 Wall pressure distributions of steady flow

Unsteady flow

The computation of an oscillating turbulent flow over the backward-facing step, where the free-stream velocity has been perturbed by a sinusoidal fluctuation is now considered. The amplitude of the oscillation was taken to be 12% of the mean velocity, and the frequency of the oscillation was varied from 0.5 to 12 Hz to investigate the effects of the unsteadiness on the general behaviour of the separated flow and the turbulence structure.

The expansion ratio of the channel was chosen to be 1:6.3 in order to compare with the experimental measurements[10]. The free-stream velocity was taken as:

$$U_0 = \bar{U}_0 + \tilde{U}_0 \sin(2\pi F)t \tag{14}$$

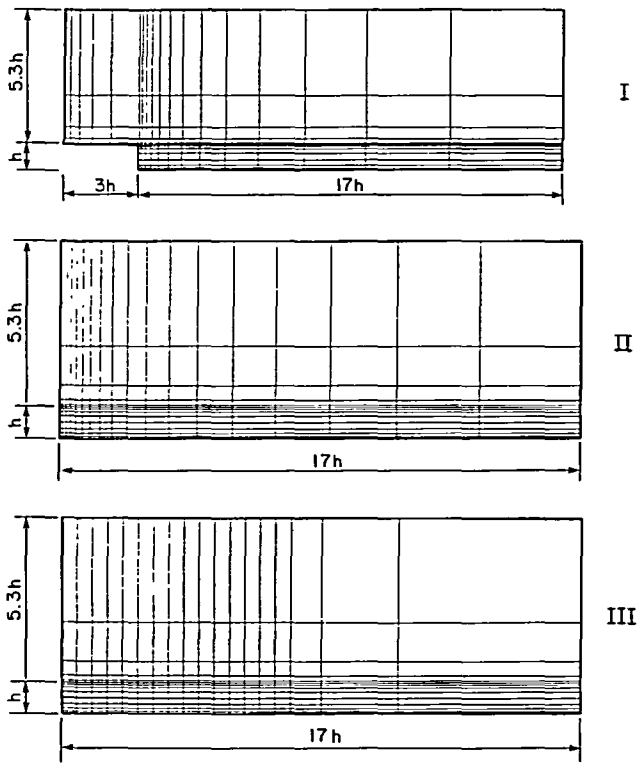

Figure 6 Finite element grids for unsteady flow

where the mean velocity $\bar{U}_0 = 1.43$ m/sec, the amplitude of the oscillating component $\tilde{U}_0 = 0.172$ m/sec and the frequency $F = 0.5 \sim 12$ Hz.

The unsteady calculations were carried out for the three different finite element grids shown in *Figure 6*. Grid I was introduced to check the effect of inlet conditions by modelling the region upstream of the step by 3 h, and thereby moving the boundary condition upstream. This grid was relatively coarse with only 181 elements in total. Grid II with 234 elements is essentially the same as the one used for the steady problem suitably modified for the different aspect ratio of the step to channel size. Grid III has the same number of elements as Grid II, but the x-dimension of the elements in the backflow region has been taken as uniform. This grid was introduced to check on the sensitivity of the results in this region to grid spacing.

Some exploratory unsteady calculations were performed using Grid I with and without the upstream portion of the grid included. It was found that including the upstream portion of the grid had very little effect on the solution downstream of the step. Hence, thereafter this upstream portion was ignored and only results from Grids II and III are reported herein. The results from Grids II and III were essentially the same for low frequencies ($F \leqslant 6$). However, it is worth noting that the calculations on Grid III were the most stable and led to the highest attainable frequency. In particular, Grid II failed to yield converged results above $F = 6$. Finally, we note that it would have been desirable to use a finer grid to check on grid dependency but this was not possible with the present computer capacity and financial resource limitations.

To test the new periodic solution program, steady flow ($F = 0$) was calculated first using Grid II. The computed velocity profiles and the normalized pressure distributions on the wall

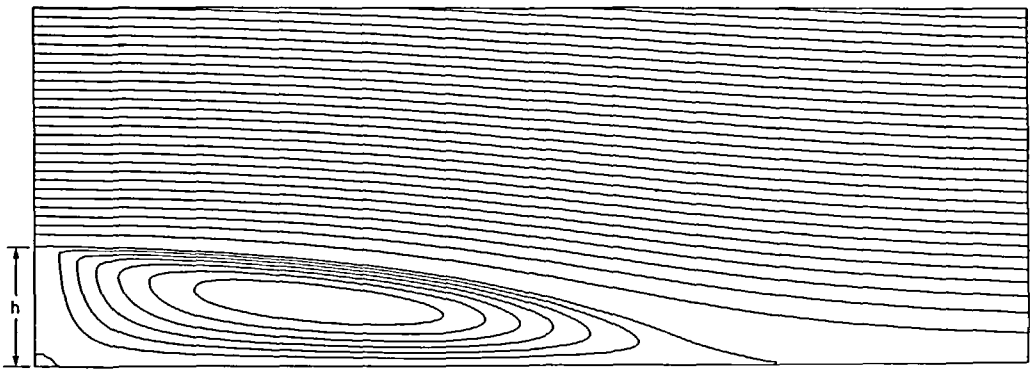

Figure 7 Streamline contours of steady flow with aspect ratio 1:6.3

were all found to be very similar to those from the previous example. The computed reattachment length, $X_r = 6.3$ h, was slightly smaller than from the previous example, because the reattachment length is dependent on the step expansion ratio[1]. *Figure 7* shows the streamline contours from this calculation, which are clearly very similar to those of *Figure 3*.

The first unsteady calculations were carried out at the low frequency of $F = 1$ Hz, since the main experimental results correspond to this case. Some typical results obtained from Grid II are shown in *Figures 8* to *11*.

The streamline contours for the mean flow and the instantaneous flows at 0, 1/4, 1/2 and 3/4 cycle points through 1 cycle of oscillation (phase angles $\phi = 0$, 90°, 180°, 270°) are shown in *Figure 8*. It is seen that the reattachment point oscillates about the mean position by about 10% (not exactly symmetrically). This is consistent with the experimental observations[10], which unfortunately were only qualitative. The computed streamline contours showed no evidence of vortex shedding, whereas the experimenters did report vortex shedding at this frequency but again only in a qualitative manner. Perhaps the finite element grid was too coarse to capture the low strength vortex shedding expected at this low frequency, because the computed results did yield what we interpreted as vortex shedding at higher frequencies.

Figure 9 shows the computed velocity profiles at various streamwise locations $x = 0.5$, 1.5, 3, 4.5 and 5.5 h and phase angles, 0°, 90°, 180° and 270° for the frequency $F = 1$. The corresponding experimental results are reproduced in *Figure 10*. It may be seen that whereas the computed results exhibit smooth changes with both changes in location and phase, the experimental ones show rather discontinuous ones. For example, the experimental profiles at locations 3 and 4.5 h exhibit almost completely opposite changes with phase. Perhaps these changes were associated with vortex shedding, but there is no explanation given in Reference 10.

The computed pressure distributions on the wall are shown in *Figure 11* for various phase angles over one cycle of oscillation. Again, some significant variation is seen to occur over the cycle. Unfortunately, the corresponding experimental results were not available for comparison.

A final observation is that at low frequencies ($F < 4$) the computed mean velocity profiles and the mean wall pressure distribution in the oscillating flow were indistinguishable from those in the steady flow. Further, the reattachment length corresponding to the mean velocity was almost the same as that for steady flow.

As the frequency was increased further, the velocity profiles and the pressure distributions were more significantly perturbed and the calculations were less stable. A larger variation in the position of rearrachment was observed and the mean reattachment length became shorter. For illustration, *Figures 12*, *13* and *14* show the velocity profiles, pressure coefficient on the wall and the streamline contours, respectively, for a frequency of $F = 5$ which corresponds to $F^* = 0.035$.

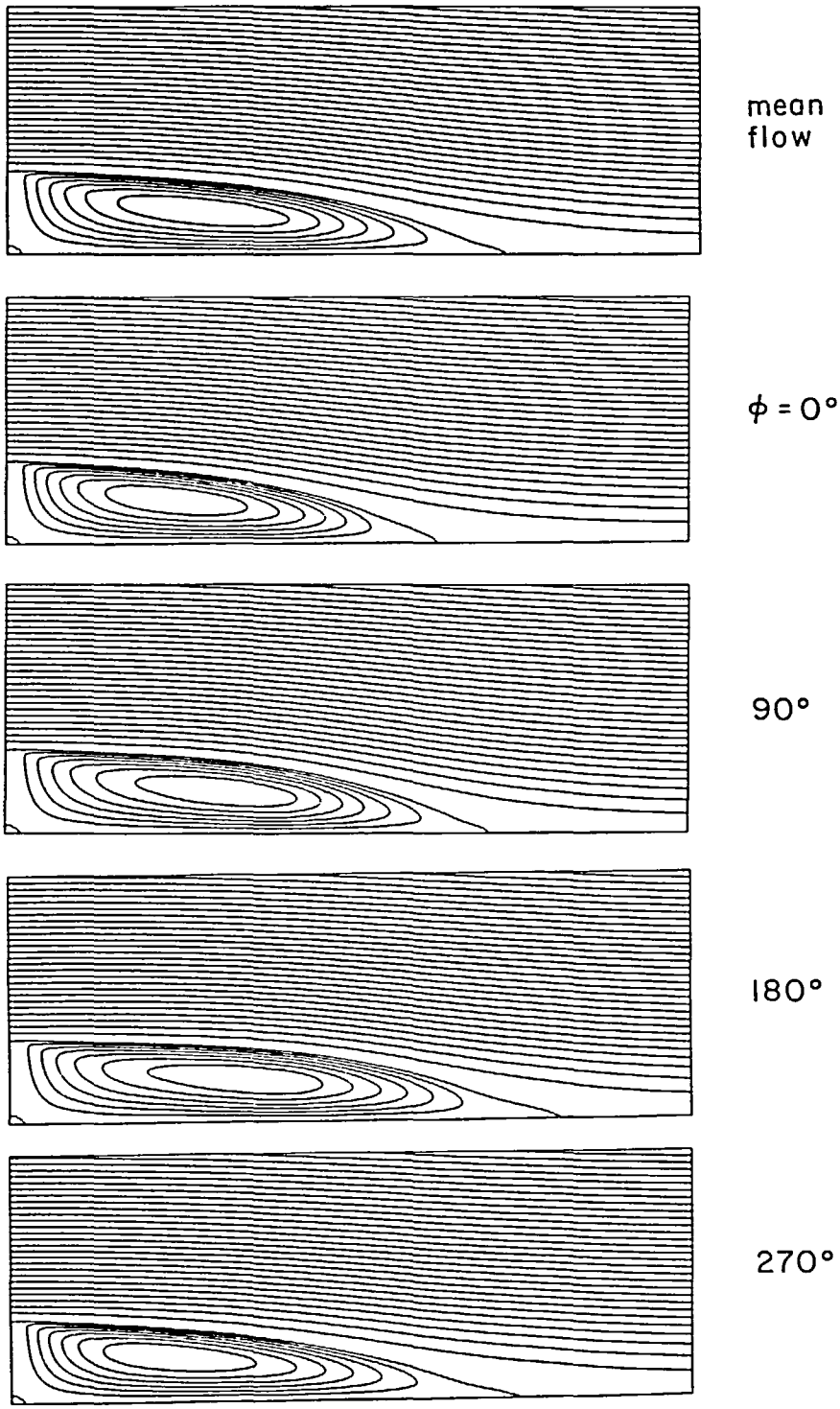

Figure 8 Streamline contours of unsteady flow at $F^* = 0.007$

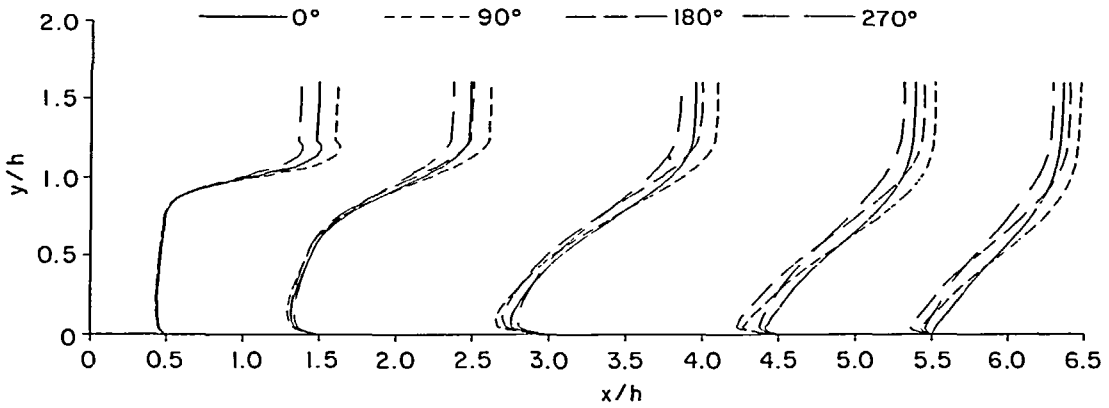

Figure 9 Velocity profiles of unsteady flow at $F^*=0.007$

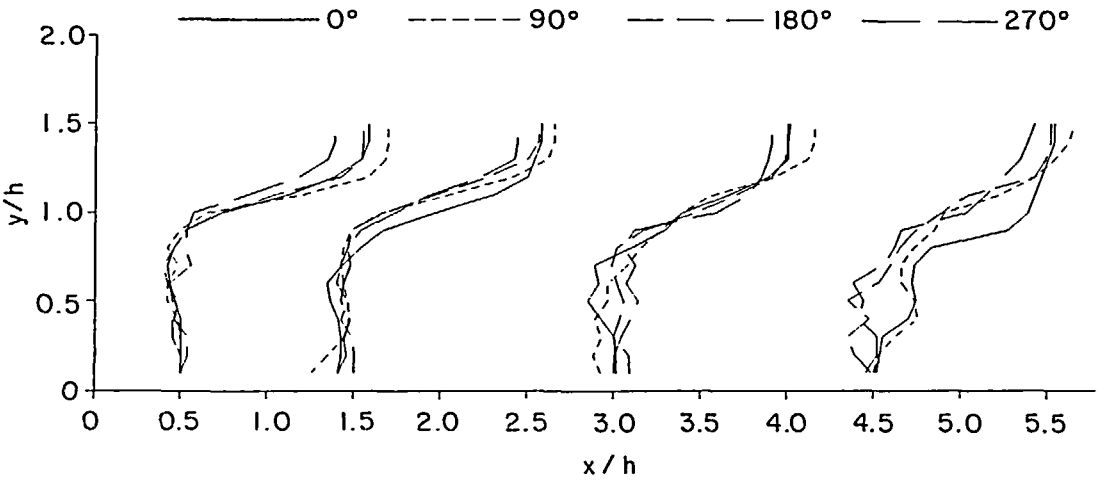

Figure 10 Experimental velocity profiles of unsteady flow at $F^*=0.007$

When the frequency was further increased, the calculations became more unstable and, in fact, Grid II failed to yield a converged solution above $F=6$. The calculations were then switched to Grid III, which were much more stable and for frequencies between 6 and 8, periodic shedding of the recirculation vortex was observable in the streamline plots. These streamline contours for each phase of the cycle became much different from those of the low frequency flows. As an example, *Figure 15* shows the streamline contours for various phases for a frequency $F=8$ ($F^*=0.056$) which is close to the reported experimental critical value of $F^*=0.07$.

One possible interpretation of these Figures is as follows: as time progresses over one cycle, the main recirculation vortex first moves downstream, elongating the recirculation region, then the main recirculation moves upstream, leaving a separate vortex adjacent to the wall which finally breaks off and moves downstream out of the main flow region. Perhaps this is the numerical equivalent of the experimental vortex shedding discussed qualitatively[10]. These results must be considered preliminary at this time, since many questions have yet to be investigated, such as grid refinement, downstream boundary conditions (the present ones are consistent with a smooth outflow, not a vortex leaving the computation region), and so on. As the frequency

was increased still further, the calculations became very unstable. The first observed symptom was that the turbulent viscosity would not converge, even though the velocity–pressure calculations did converge for constant viscosity distributions. This was probably due to the unstable property of the flow near the critical frequency ($F^*=0.07$).

Converged results were actually obtained with Grid III at frequencies above this critical value, but the results were very oscillatory in space and appeared to be non-physical. This was interpreted as indicative of insufficient grid refinement.

Some particular numerical results for the time dependent reattachment position are given in *Table 2*. The Table shows the minimum and maximum positions of this point and the associated phase angles for their occurrence as well as the position for the mean flow component as obtained

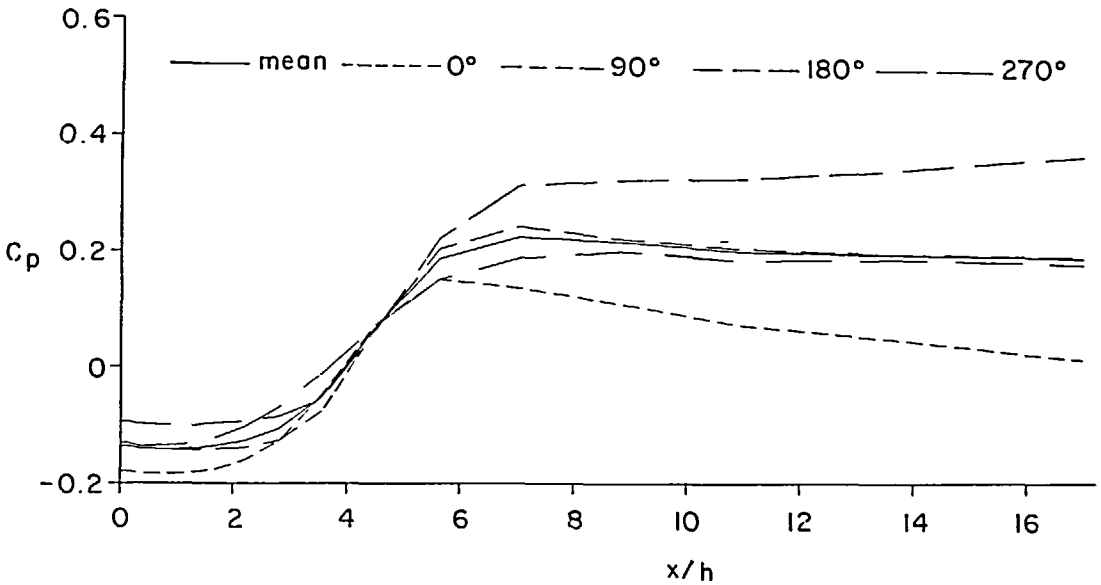

Figure 11 Wall pressure distributions of unsteady flow at $F^*=0.007$

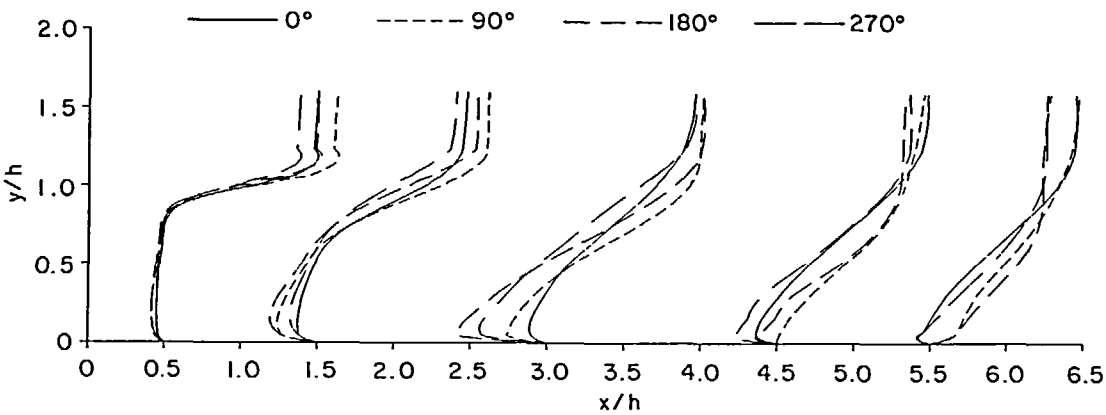

Figure 12 Velocity profiles of unsteady flow at $F^*=0.035$

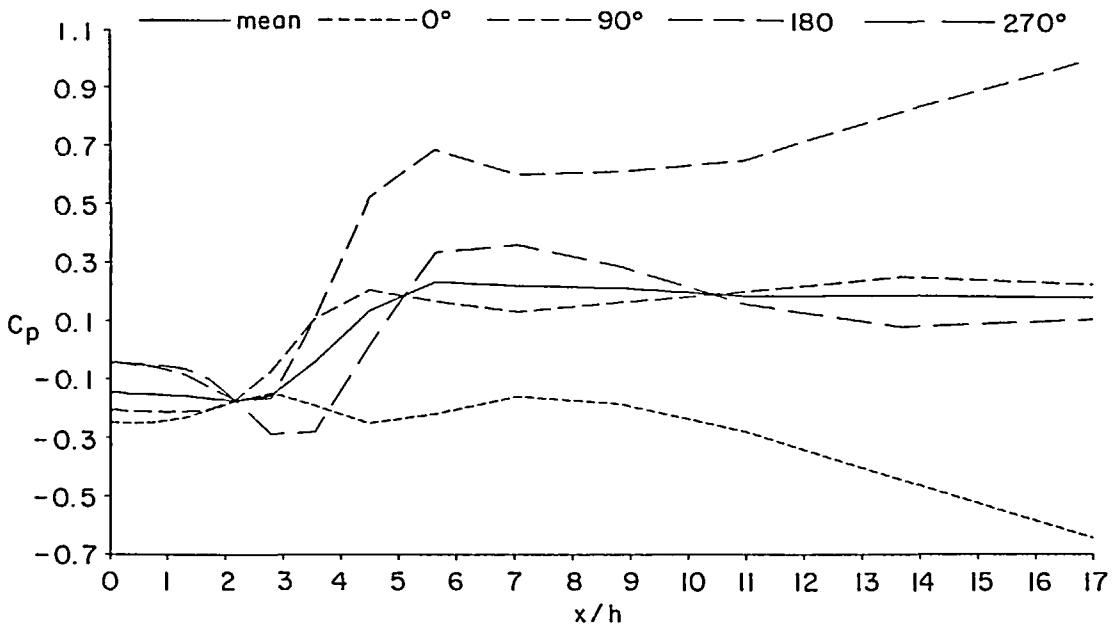

Figure 13 Wall pressure distributions of unsteady flow at $F^*=0.035$

Table 2 Numerical results for unsteady reattachment position and phase angle

Frequency		Grid III					Grid II
F(Hz)	F^*	$\frac{X_{r\min}}{h}$	$\phi_{\min}$ (deg)	$\frac{X_{r\max}}{h}$	$\phi_{\max}$ (deg)	$\frac{X_{r\text{mean}}}{h}$	$\frac{X_{r\text{mean}}}{h}$
0.5	0.0035	4.90	310	6.66	172	5.36	6.33
1.0	0.007	4.84	336	6.97	210	5.39	6.13
2.0	0.014	4.72	4	7.33	258	5.37	6.13
4.0	0.028	4.10	34	6.82	344	5.32	5.70
6.0	0.042	4.11	80	6.53	66	5.22	5.08
8.0	0.056	4.51	158	6.63	116	4.99	—
10.0	0.07	4.39	214	7.45	186	4.92	—

from Grid III. The corresponding mean flow results as obtained from Grid II are also shown for comparison. According to the former results, the mean flow position is essentially independent of frequency, at least up to $F=6$. The fact that the corresponding Grid II results show more frequency dependency is probably due to the grid design. On the other hand, the results for the minimum and maximum position do exhibit a frequency dependence, namely, that the size of the excursions from the mean increase with frequency and the phase angles also increase with frequency. It appears that these minimum and maximum positions occur later in the cycle as the frequency increases. This is analogous to the behaviour of a damped oscillator for frequencies below resonance. The results for the higher frequencies ($F=8$ and 10) are subject to interpretation, in that they were obtained from only the most upstream part of the recirculating flow (see e.g. *Figure 15*).

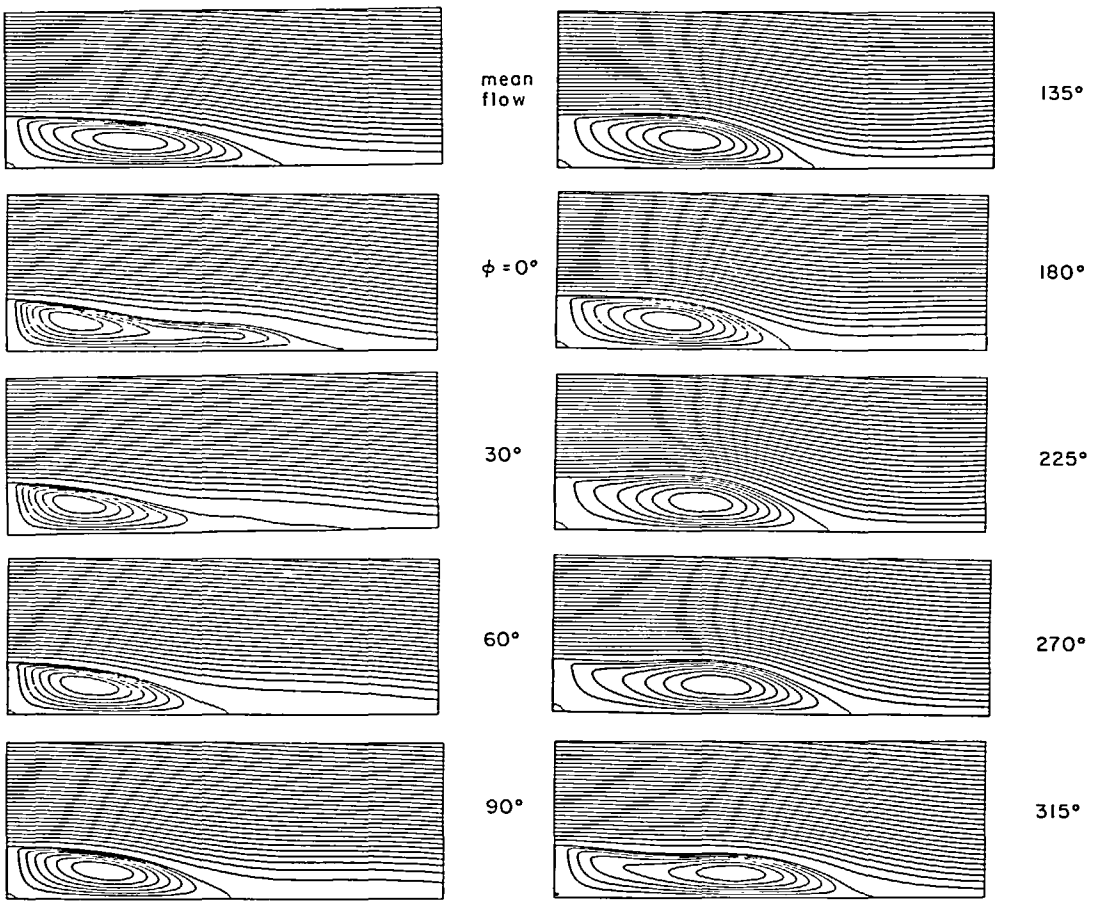

Figure 14 Streamline contours of unsteady flow at $F^* = 0.035$

CONCLUSIONS

The main thrust of this work was to test the potential of using a periodic solution technique along with an algebraic closure model to simulate turbulent flows with substantial separated-reattaching flow regions. The example of flow over a backward-facing step was chosen as the test case because of its popularity and the availability of comparison results.

The results obtained for the steady flow case compared well with other results, thereby providing credibility to the modified Baldwin–Lomax algebraic closure model's capability of representing separated-reattaching flows.

The results for the oscillating flow case appeared to have many of the correct physical features. For example, for low relative amplitudes of the oscillating component and low frequencies, the mean component of the flow was very similar to that of the steady flow case. Further, the reattachment point was observed to oscillate about a mean position just as reported in the experiment. No vortex shedding was detectable in the numerical results at low frequency, but as the frequency was increased towards the critical value reported in the experiment, the nature of the numerical results did change and the instantaneous streamlines began to exhibit a phenomenon which could be interpreted as 'vortex shedding'. Further, the stability of the

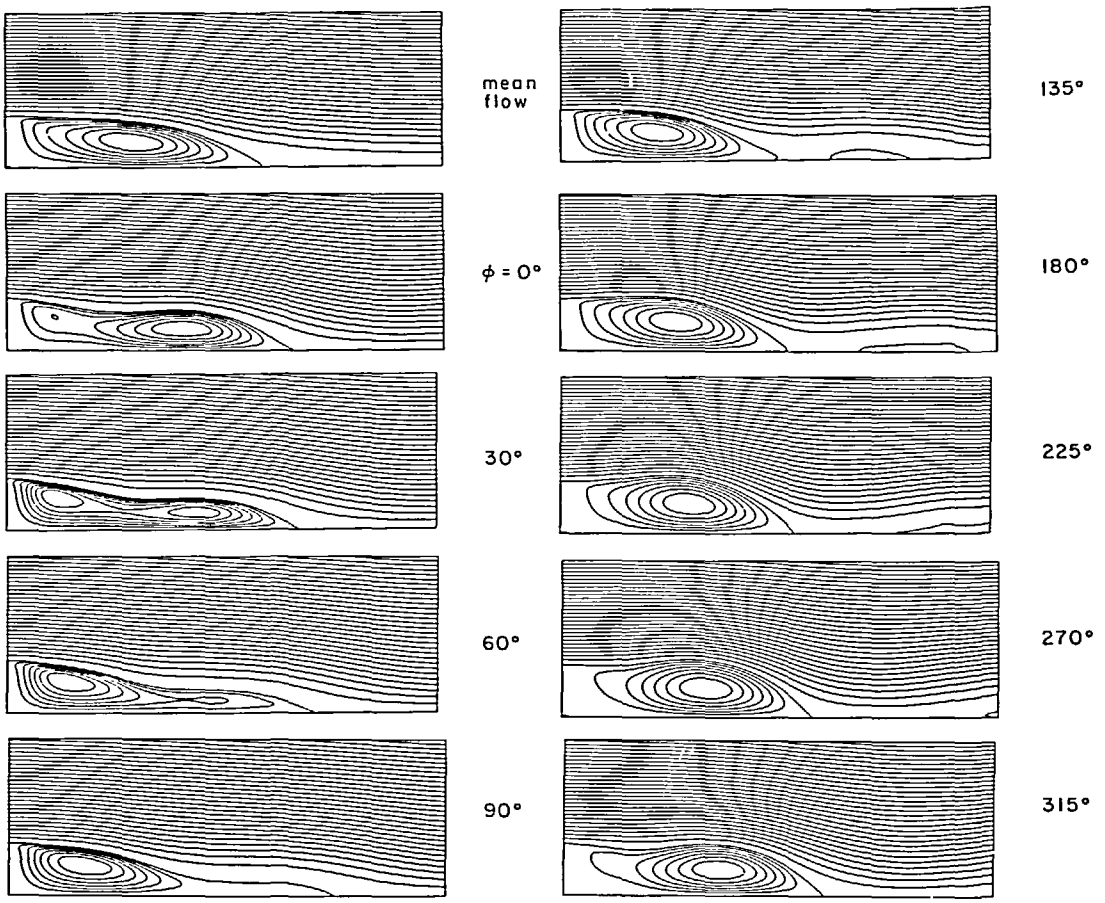

Figure 15 Streamline contours of unsteady flow at $F^* = 0.056$

calculations deteriorated significantly as well. The stability of the calculations improved again for frequencies above the critical one but the accuracy of the results was suspect.

In conclusion, we can say that the modified Baldwin–Lomax eddy viscosity model seems to be appropriate for the type of separated flow configuration considered in the present work. The method of averaging appears to work well to obtain periodic solutions of time-dependent flows and results in significant savings over time integration methods. In the present work, the turbulent viscosity was held constant and depended only on the mean component of the flow. It would be interesting to speculate on the possibility of including a periodic component of the viscosity which presumably would be dependent on the periodic components of the flow. The present results have to be considered preliminary, but even so are sufficient to show the potential of the present approach and that it is worthy of further investigation.

The present periodic solution approach should be more cost effective than time integration even though the procedure does require the solution of about three times more variables. Unfortunately at this time there is no direct way to compare the two without direct simulation of both approaches.

ACKNOWLEDGEMENTS

This work has been supported by the Canadian Natural Sciences and Engineering Research Council.

REFERENCES

1 Simpson, R. L. Two-dimensional turbulent separated flow, *AGARDograph 287*, **1** (1985)
2 Simpson, R. L. Turbulent boundary-layer separation, *A. Rev. Fluid Mech.*, **21**, 205–234 (1989)
3 *Proc. 1980–1981 AFOSR–HTTM-Stanford Conf. Complex Turbulent Flows: Comparison of Computation and Experiment*, Vol. I and II (1982)
4 Kim, J., Kline, S. J. and Johnston, J. P. Investigation of a reattaching turbulent shear layer: flow over a backward-facing step, *J. Fluid Eng., ASME Trans.*, **102**, 302–308 (1980)
5 Troutt, T. R., Scheelke, B. and Norman, T. R. Organized structures in a reattaching separated flow field, *J. Fluid Mech.*, **143**, 413–427 (1984)
6 Sohn, J. L. Evaluation of FIDAP on some classical laminar and turbulent benchmarks, *Int. J. Num. Meth. Fluids*, **8**, 1469–1490 (1988)
7 Utnes, T. Two equation (k,ε) turbulence computations by the use of a finite element model, *Int. J. Num. Meth. Fluids*, **8**, 965–975 (1988)
8 Autret, A., Grandotto, M. and Dekeyser, I. Finite element computation of a turbulent flow over a two-dimensional backward-facing step, *Int. J. Num. Meth. Fluids*, **7**, 89–102 (1987)
9 Brocher, E. Oscillatory flows in ducts: a report on Euromech 73, *J. Fluid Mech.*, **79**, 113–126 (1977)
10 Mullin, T., Greated, C. A. and Grant, I. Pulsating Flow Over a Step, *Phys. Fluids*, **23**, 669–674 (1980)
11 Brooks, A. N. and Hughes, T. J. R. Streamline upwind/Petrov–Galerkin formulations for convection dominated flows with particular emphasis on the incompressible Navier–Stokes equations, *Comp. Meth. Appl. Mech. Eng.*, **32**, 199–259 (1982)
12 Qin, Z. and Olson, M. D. Finite element-algebraic closure analysis of turbulent separated-reattaching flow around a rectangular body, *Comp. Meth. Appl. Mech. Eng.*, **85**, 131–150 (1991)
13 Baldwin, B. S. and Lomax, H. Thin layer approximation and algebraic model for separated turbulent flows, *AIAA Paper 78-257* (1978)
14 York, B. and Knight, D. Calculation of two-dimensional turbulent boundary layers using the Baldwin–Lomax model, *AIAA J.*, **23**, 1849–1850 (1985)
15 Goldberg, U. C. and Chakravarthy, S. R. Prediction of separated flows with a new backflow turbulence model, *AIAA J.*, **26**, 405–408 (1988)
16 Pattani, P. G. and Olson, M. D. Finite element-algebraic closure modelling of turbulent entrance type flows, *5th Int. Conf. Laminar Turbulent Flows, Montreal* (Eds. C. Taylor *et al.*), Pineridge Press, Swansea, pp. 386–397 (1987)
17 Telionis, D. P. and Tsahalis, D. Th. Unsteady turbulent boundary layers and separation, *AIAA J.*, **24**, 468–474 (1976)
18 Cousteix, J., Desopper, A. and Houdeville, R. Structure and development of a turbulent boundary layer in an oscillatory external flow, *Turbulent Shear Flow*, **1**, 154–171 (1977)
19 Cebeci, T. and Carr, L. W. Prediction of boundary layer characteristics of an oscillating airfoil, *Unsteady Turbulent Shear Flows*, 145–158 (1981)
20 Cebeci, T. Unsteady separation, *Symp. Num. Phys. Aspects Aerodyn. Flows*, Cal. State Univ., Springer Verlag, New York (1981)
21 Qin, Z. and Olson, M. D. Periodic solution of turbulent oscillating channel flow, *Int. J. Num. Meth. Fluids*, submitted (1990)
22 Goldberg, U. C. Separated flow treatment with a new turbulence model, *AIAA J.*, **24**, 1711–1713 (1986)
23 Pattani, P. G. and Olson, M. D. Periodic solutions of rigid body-viscous flow interaction, *Int. J. Num. Meth. Fluids*, **7**, 653–696 (1987)

APPENDIX

Details of matrices in (4) and (7)

$$\mathbf{d}=[u_1u_2\ldots u_8v_1v_2\ldots v_8p_1p_2p_3p_4]^{\mathrm{T}}$$

$$\mathbf{A}=[A_1^uA_2^u\ldots A_8^uA_1^vA_2^v\ldots A_8^vA_1^pA_2^pA_3^pA_4^p]^{\mathrm{T}}$$

$$\mathbf{B}=[B_1^uB_2^u\ldots B_8^uB_1^vB_2^v\ldots B_8^vB_1^pB_2^pB_3^pB_4^p]^{\mathrm{T}}$$

$$\mathbf{C}=[C_1^uC_2^u\ldots C_8^uC_1^vC_2^v\ldots C_8^vC_1^pC_2^pC_3^pC_4^p]^{\mathrm{T}}$$

$$\mathbf{M}=\begin{bmatrix} M_{ij} & 0 & 0 \\ 0 & M_{ij} & 0 \\ 0 & 0 & 0 \end{bmatrix}$$

where

$$M_{ij}=\iint_{Ae}\rho W_i N_j \,\mathrm{d}A \qquad i,j=1,2,\ldots,8$$

$$\mathbf{K}=\begin{bmatrix} K_{ij}^{uu} & K_{ij}^{uv} & K_{ij}^{up} \\ K_{ij}^{vu} & K_{ij}^{vv} & K_{ij}^{vp} \\ K_{ij}^{pu} & K_{ij}^{pv} & 0 \end{bmatrix}$$

where

$$K_{ij}^{uu}=\iint_{Ae}\mu_e(2N_{i,x}N_{j,x}+N_{i,y}N_{j,y})\mathrm{d}A$$

$$K_{ij}^{uv}=\iint_{Ae}\mu_e N_{i,y}N_{j,x}\,\mathrm{d}A=K_{ji}^{vu} \qquad i,j=1,2,\ldots,8$$

$$K_{ij}^{vv}=\iint_{Ae}\mu_e(2N_{i,y}N_{j,y}+N_{i,x}N_{j,x})\mathrm{d}A$$

$$K_{ij}^{up}=\iint_{Ae}N_i M_{j,x}\,\mathrm{d}A \qquad i=1,2,\ldots,8 \quad j=1,2,3,4$$

$$K_{ij}^{vp}=\iint_{Ae}N_i M_{j,y}\,\mathrm{d}A \qquad i=1,2,\ldots,8 \quad j=1,2,3,4$$

$$K_{ij}^{pu}=\iint_{Ae}M_i N_{j,x}\,\mathrm{d}A \qquad i=1,2,3,4 \quad j=1,2,\ldots,8$$

$$K_{ij}^{pv}=\iint_{Ae}M_i N_{j,y}\,\mathrm{d}A \qquad i=1,2,3,4 \quad j=1,2,\ldots,8$$

$$\delta=\begin{Bmatrix} \delta_{ijk}^{x}u_j u_k+\delta_{ijk}^{y}v_j u_k \\ \delta_{ijk}^{x}u_j v_k+\delta_{ijk}^{y}v_j v_k \\ 0 \end{Bmatrix}$$

where

$$\delta_{ijk}^{x}=\iint_{Ae}\rho W_i N_j N_{k,x}\,\mathrm{d}A \qquad i,j,k=1,2,\ldots,8$$

$$\delta_{ijk}^{y}=\iint_{Ae}\rho W_i N_j N_{k,y}\,\mathrm{d}A$$

$$\delta_A=\begin{Bmatrix} \delta_{ijk}^{x}(A_j^u A_k^u+B_j^u B_k^u/2+C_j^u C_k^u/2)+\delta_{ijk}^{y}(A_j^v A_k^u+B_j^v B_k^u/2+C_j^v C_k^u/2) \\ \delta_{ijk}^{x}(A_j^u A_k^v+B_j^u B_k^v/2+C_j^u C_k^v/2)+\delta_{ijk}^{y}(A_j^v A_k^v+B_j^v B_k^v/2+C_j^v C_k^v/2) \\ 0 \end{Bmatrix}$$

$$\delta_B=\begin{Bmatrix} \delta_{ijk}^{x}(A_j^u B_k^u+A_k^u B_j^u)+\delta_{ijk}^{y}(A_j^v B_k^u+A_k^u B_j^v) \\ \delta_{ijk}^{x}(A_j^u B_k^v+A_k^v B_j^u)+\delta_{ijk}^{y}(A_j^v B_k^v+A_k^v B_j^v) \\ 0 \end{Bmatrix}$$

$$\delta_C=\begin{Bmatrix} \delta_{ijk}^{x}(A_j^u C_k^u+A_k^u C_j^u)+\delta_{ijk}^{y}(A_j^v B_k^u+A_k^u C_j^v) \\ \delta_{ijk}^{x}(A_j^u C_k^v+A_k^v C_j^u)+\delta_{ijk}^{y}(A_j^v C_k^v+A_k^v C_j^v) \\ 0 \end{Bmatrix}$$